*Iran J Public Health, Vol. 52, No. 9, Sep 2023, pp.1902-1916*

**Original Article**

# Expression and Prognostic Value of m6A RNA Methylation-Related Genes in Thyroid Cancer

***Hui Han [1], Xiaodan Fu [2], Yu Zhang [3], Dingcun Luo [3], Xianfeng Zhang [2], *Xiaohong Wu [4]***

1. *Department of Endocrinology, the Affiliated Hangzhou Hospital of Nanjing Medical University, Hangzhou, Zhejiang, China*
2. *Department of Endocrinology, Affiliated Hangzhou First People's Hospital, Zhejiang University School of Medicine, Hangzhou, Zhejiang, China*
3. *Department of Surgical Oncology, Affiliated Hangzhou First People's Hospital, Zhejiang University School of Medicine, Hangzhou, Zhejiang, China*
4. *Department of Endocrinology, The First Affiliated Hospital with Nanjing Medical University, Nanjing, Jiangsu, China*

***Corresponding Author:** Email: drxhwu@njmu.edu.cn

**(Received 10 Feb 2023; accepted 19 May 2023)**

**Abstract**

**Background:** N6-methyladenosine (m6A) methylation modification is involved in tumorigenesis and progression and can affect various stages of RNA processing. We aimed to determine m6A methylation modifications on a transcriptome-wide scale in thyroid cancer.

**Methods:** RNA samples from cancerous tissues and adjacent tissues extracted from patients with papillary thyroid carcinoma (PTC) from Hangzhou First People's Hospital, Zhejiang, China from January 2019 to January 2020 were used for m6A-sequencing. The biological function of differentially expressed genes (DEGs) was analyzed via Gene Ontology (GO) and Kyoto Encyclopedia of Genes and Genomes (KEGG) analysis. Correlation analysis between the results of transcriptome sequencing and m6A-sequencing was also performed. The key m6A immune-related genes were downloaded from Immport. LASSO regression was performed on the resulting genes to establish a prognostic risk model, which was verified by multivariate Cox proportional hazards regression analyses, receiver operating characteristic (ROC) curves and Kaplan-Meier survival analysis.

**Results:** An increase in m6A content in the total RNA of PTC was observed. A total of 123 genes with significant differential expression and differential methylation sites in thyroid cancer were selected, related to protein digestion and absorption, linoleic acid metabolism, legionellosis and alpha-linolenic acid metabolism. Seven genes (*GDNF*, *EBI3*, *CCL2*, *BMP5*, *TGFB2*, *CGB3* and *RLN2*) were found to be predictive of PTC.

**Conclusion:** We analyzed the expression, enrichment pathways and functions of m6A methylation-related genes in the whole transcriptome of thyroid cancer and provided a prognostic risk model for thyroid cancer patients.

**Keywords:** Thyroid cancer; N6-methyladenosine; Methylated RNA immunoprecipitation sequencing

## Introduction

Thyroid cancer is one of the most common endocrine-related malignancies, and in recent years, the incidence of thyroid cancer worldwide has increased rapidly, and thyroid cancer in China is reported to increase at a rate of 20% (1, 2). Although surgery, radiotherapy and levothyroxine treatment methods continue to improve, more than 10% of thyroid cancer patients still relapse

and current treatment methods have limited effects on the local progression and distant metastasis of thyroid cancer (3,4). Therefore, further clarification of the molecular mechanism of thyroid cancer is helpful to the prognosis and treatment of patients with thyroid cancer.

N6-methyladenosine (m6A) methylation modification is one type mRNA modification in higher eukaryotes (5). There are three types of proteins that jointly maintain the balance of the m6A network, namely the methyltransferase complex, demethylase and m6A binding protein (6). Among them, the methyltransferase complex includes METL3, METL14 and WTAP, and the demethylase is composed of FTO and ALKBH5. mRNA m6A modification closely influenced tumor occurrence and development (7). m6A is an important factor in regulating tumor occurrence and development, and its expression level has a decisive effect on the pathological development of tumors. It has been found that m6A modification is implicated in various kinds of tumors, including liver cancer, glioblastoma, pancreatic cancer and acute myeloid leukemia (8). In the regulation of cancer-related gene expression, m6A can promote or inhibit the growth and invasion of tumor cells and is also closely implicated in the sensitivity of cancer cells to chemotherapy and radiotherapy (9). However, the role of m6A modification in thyroid cancer needs to be further explored.

Therefore, we used m6A immunoprecipitation and epitranscriptome chip technology to detect the differential modification of m6A methylation of mRNA in normal tissues and thyroid cancer tissues, and on this basis, explore the epigenetic factors affecting thyroid cancer.

## Materials and Methods

### *Collection of samples*

Cancer tissue (n = 3) and paracancerous tissue (n = 3) of PTC patients were obtained from Hangzhou First People's Hospital, Zhejiang, China from January 2019 to January 2020. The patients inclusion criteria were: 1) had confirmed pathological diagnosis of PTC, 2) did not have other malignancy apart from PTC, 3) did not undergo any neoadjuvant therapy prior to tissue sampling, 4) signed informed consent.

The study exclusion criteria were: 1) age younger than 18 years old and older than 80- years old, 2) pregnant or breast feeding.

All subsequent research was approved by the Ethics Committee of Hangzhou First People's Hospital (2018-146-01).

### *RNA isolation and purification*

Total RNA in the tissues was extracted with the Total RNA Extraction Kit (DP419, Tiangen, China). The amount, purity and integrity of RNA were examined using NanoDrop ND-1000 (NanoDrop, USA), Bioanalyzer 2100 (Agilent, USA) and agarose gel electrophoresis.

### *RNA m6A quantification*

The m6A content in the total RNA was measured using the m6A RNA Methylation Assay (ab185912, Abcam, UK). After mixing with the binding solution, the negative control, positive control and RNA samples were reacted with capture antibody, detection antibody and enhancer solution. After the addition of the color developing solution, the reaction was terminated when the positive control color turned to medium blue. The absorbance value was measured at a wavelength of 450 nm with a microplate reader (Multiskan MK3, Thermo Fisher, USA). The calculation method of m6A in total RNA (%) is consistent with a previous study (10).

### *m6A immunoprecipitation*

The mRNA captured by Dynabeads Oligo (dT) (25-61005, Thermo Fisher) was fragmented by Magnesium RNA Fragmentation Module (E6150S, NEB, USA) with the conditions of 86℃ for 7 minutes. Fragmented RNA, immunomagnetic beads (14311D, Thermo Fisher) and m6A antibody (202003, Synaptic Systems, Germany) were mixed in IP buffer (50 mM Tris-HCl, 750 mM NaCl and 0.5% Igepal CA-630) to perform IP.

### Sequencing

The product of IP was reverse transcribed into cDNA under the action of reverse transcriptase (1896649, Thermo Fisher). The DNA and RNA compound double strands were converted into DNA double strands with the help of *E. coli* DNA polymerase I (m0209, NEB) and RNase H (m0297, NEB). dUTP Solution (R0133, Thermo Fisher) was used to fill the ends of double-stranded DNA. A base was added at each end of the chain so that it could be connected to a linker with a T base at the end. UDG enzyme (m0280, NEB) and PCR reaction were conducted to obtain a library with a fragment size of 300bp ± 50bp. Finally, we used Illumina Novaseq™ 6000 (LC Bio-Technology CO., Ltd. China) to perform paired-end sequencing with the sequencing mode set to PE150.

### Bioinformatics Analysis

The raw data (IP samples and Input samples) were subjected to quality control using Fastp (https://github.com/OpenGene/fastp). The obtained clean data (fastq format) were aligned to the genome (Latin: Homo sapiens, genome version: v96) using HISAT2 (http://daehwankimlab.github.io/hisat2). Afterward, peak calling analysis and genetic difference peak analysis was performed with the R package exomePeak (https://bioconductor.org/packages/exomePeak). The tdf or bigwig format files were visually displayed by the IGV software (http://www.igv.org). The peak annotation, motif analysis, gene assembly and quantification were performed using ChIPseeker (https://bioconductor.org/packages/ChIPseeker), MEME2 (http://meme-suite.org), HOMER (http://homer.ucsd.edu/homer/motif) and StringTie (https://ccb.jhu.edu/software/stringtie). The quantification method was FPKM (total exon fragments/mapped reads [millions] × exon length [kB]), and the R package edgeR (https://bioconductor.org/packages/edgeR) was used for difference analysis. Fold change (FC) ≥ 2 or FC ≤ 0.5 and p-value ≤ 0.05 was used as the threshold for differential gene screening, and lastly, 123 differential genes were obtained. The biological function of DEGs was analyzed by GO analysis and KEGG signaling pathways analysis.

### Construction of a prognostic signature

Transcriptome expression data of thyroid cancer were downloaded from TCGA database (https://cancergenome.nih.gov/) using the R package GDCRNATools to make a heat map of the selected genes (n=153). The immune-related genes were downloaded from Immport (https://www.immport.org/home) and intersected with the selected 153 genes to obtain 36 genes. These genes were entered into LASSO Cox regression analysis to obtain 7 genes, which were then incorporated into the coxph multivariate risk model, and risk scoring was performed on each sample. The data were divided into a high-risk group and a low-risk group according to the median cutoff value of the risk score. The Kaplan-Meier survival method was used to assess the applicability of the prognostic model, and the ROC curve was used to assess accuracy of the predictive models for 3/5/10-year OS.

### Statistical analyses

All statistical analyses were implemented performed using thewith SPSS software v16.0 (Chicago, IL, USA). The results were visualized by Graphpad Prism 9.0 or R software. Most analyses were performed using R software. The t-test is used to analyze the differences between the two groups. Statistical significance was set at probability values of $P < 0.05$.

## Results

### Characteristics of m6A-sequencing data

We performed m6A sequencing on clinical tissues from three PTC patients. The content of m6A in total RNA of PTC tissues (Cancer) was significantly higher than corresponding adjacent tissues (Normal) (Fig. 1A-B, $P<0.05$).

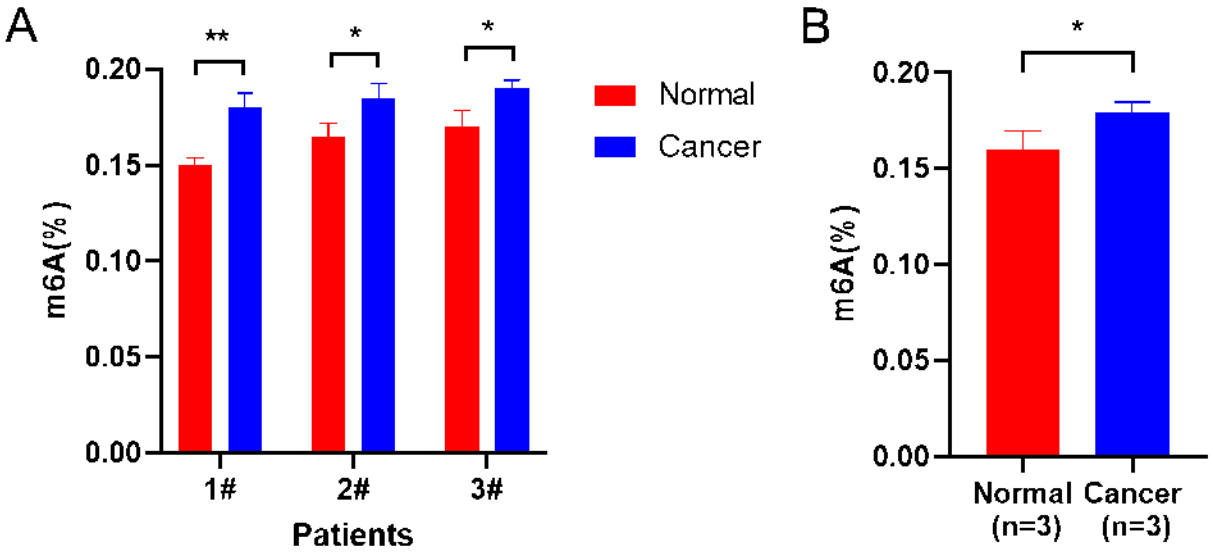


**Fig. 1: m6A levels in the total RNA isolated from cancer and adjacent (Normal) tissues of PTC.**
A, Illustration of m6A levels in the total RNA in Cancer tissues and Normal tissues of 3 PTC patients indivudually. B, Upon separately combining the m6A levels from the two groups of tissues, we observed a significant increase in the overall level of m6A in total RNAs isolated from PTC tissues compared with Normal tissues. *$P$<0.05 and **$P$<0.01

Then we calculated the effective sequencing amount of Q20, Q30 and GC content in the cleaned data (Table 1). Figure 2 shows the statistics of the proportional distribution of exons, introns and intergenic regions after the data was compared to the genome. The sequence location percentage of each sample in the exon region was greater than 90%, indicating that the sequencing result was reasonable.

**Table 1:** Illustration of the comparison of the genome in each sample from three patients

| *Sample_ID* | *Raw_Reads* | *Raw_Bases* | *Valid_Reads* | *Valid_Bases* | *Valid%* | *Q20%* | *Q30%* | *GC%* |
|---|---|---|---|---|---|---|---|---|
| NT_1_IP | 38546408 | 5.78G | 37486578 | 5.23G | 90.40 | 98.04 | 93.93 | 50.98 |
| CT_1_IP | 50002786 | 7.50G | 48788136 | 6.78G | 90.39 | 97.86 | 93.62 | 51.03 |
| NT_2_IP | 38513854 | 5.78G | 37602792 | 5.25G | 90.81 | 98.00 | 93.90 | 51.78 |
| CT_2_IP | 52851652 | 7.93G | 51558480 | 7.21G | 90.90 | 98.09 | 94.12 | 51.11 |
| NT_3_IP | 49808302 | 7.47G | 48468722 | 6.75G | 90.38 | 98.10 | 94.19 | 51.09 |
| CT_3_IP | 50070556 | 7.51G | 48894842 | 6.82G | 90.76 | 98.04 | 94.03 | 51.35 |
| NT_1_input | 53706732 | 8.06G | 52951928 | 7.38G | 91.60 | 98.45 | 94.98 | 49.87 |
| CT_1_input | 46810404 | 7.02G | 46167786 | 6.37G | 90.74 | 98.07 | 94.10 | 49.69 |
| NT_2_input | 33166884 | 4.98G | 32693814 | 4.54G | 91.31 | 98.27 | 94.55 | 50.79 |
| CT_2_input | 38848408 | 5.83G | 38408024 | 5.31G | 91.15 | 98.32 | 94.64 | 50.49 |
| NT_3_input | 36715588 | 5.51G | 36228502 | 5.01G | 91.02 | 98.28 | 94.56 | 49.68 |
| CT_3_input | 33392204 | 5.01G | 33011082 | 4.57G | 91.17 | 98.23 | 94.42 | 49.39 |

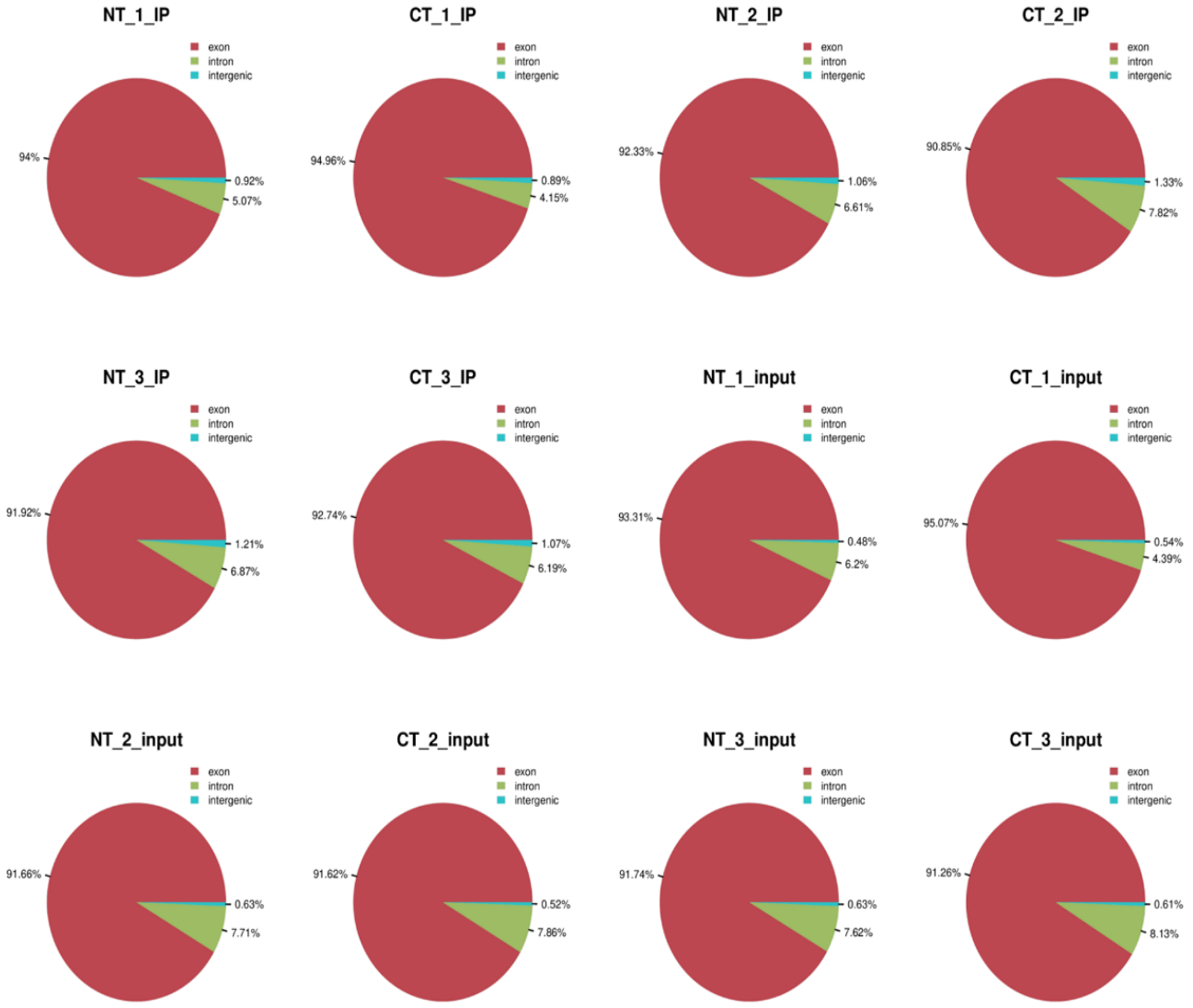


**Fig. 2: A statistical chart of the proportional distribution of each sample from three patients in the corresponding exon, intron, and intergenic regions.** IP: Immunoprecipitation Input was regarded as the internal control. NT: Normal tissue. CT: Cancer tissue

### *Peak calling and difference peak analysis*

The R package exomepeak2 was used to scan the whole gene range and analyze the difference in peak calling. We divided the gene into three segments: 5'UTR, CDS and 3'UTR and counted the distribution of peak in each segment (Fig. 3A). Then, all the samples were put together to show the degree of enrichment of the data near the transcription start site (TSS) of the gene transcriptome (Fig. 3B). The *P*-value less than 0.05 was used as the threshold to screen the differential genes, based on which 1417 differential m6A were identified, and the differential peak was annotated with a chipseeker. The distribution of the peaks in each segment and the distribution of transcription factor-binding loci relative to TSS are shown in Fig. 4A-B.

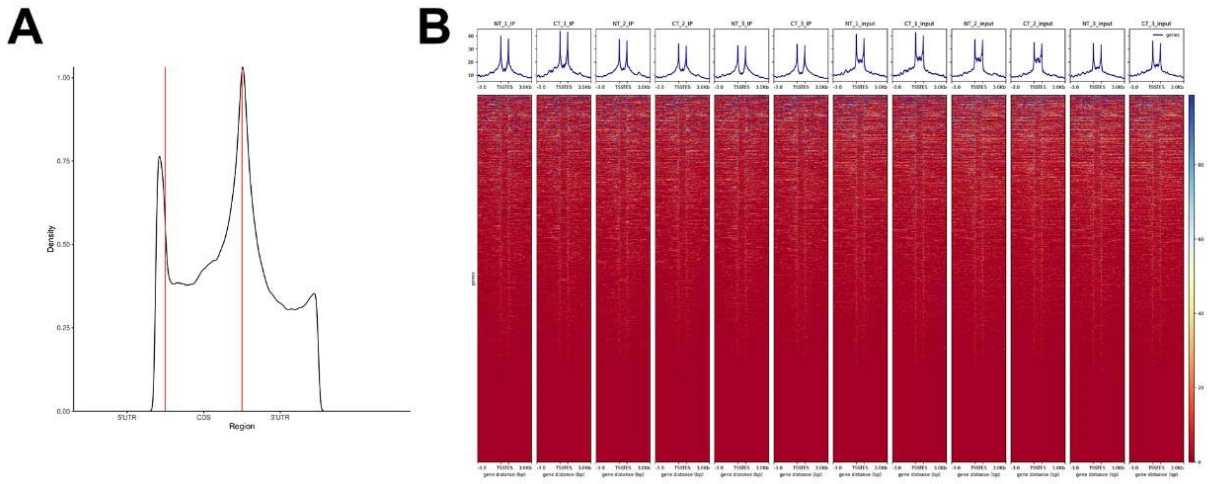


**Fig. 3: Enrichment of m6A peaks along the transcripts.**
A, Each transcript is divided into three parts: 5'UTR, CDS and 3'UTR. B, The degree of enrichment of all samples near the transcription start and end site of the gene transcriptome. UTR: untranslated region. CDS: coding sequence

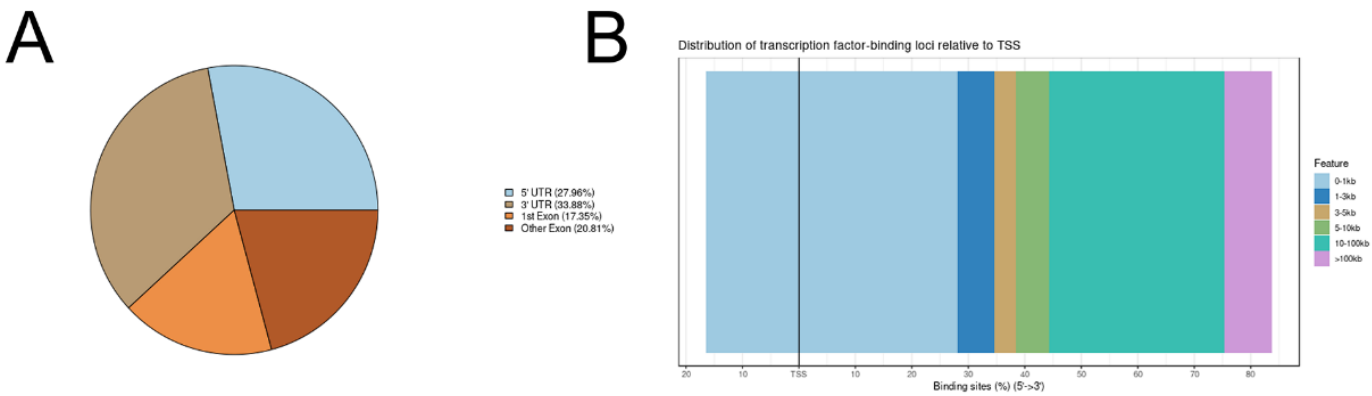


**Fig. 4: The results of differential m6A methylation peak analysis.**
A, The percentage m6A peak distribution within different gene contexts (5'UTR, 3'UTR, 1st exon, and other exons). B, The distribution of transcription factor-binding loci relative to transcription start site

### *Analysis of gene expression data*

The differentially expressed genes (DEGs) (n=123) in Cancer tissue and Normal tissue samples are shown in the Heatmap (Fig. 5A) and volcano map (Fig. 5B). We analyzed the DEGs by GO and KEGG analysis. Figure 6A depicted the enrichment of DEGs in the three categories of cellular component, molecular function, and biological process. Figure 6B showed that DEGs were related to protein digestion and absorption, linoleic acid metabolism, legionellosis and alpha-linolenic acid metabolism. Correlation analysis between the results of transcriptome sequencing and m6A-seq was performed, and drew a four-quadrant graph (Fig. 7).

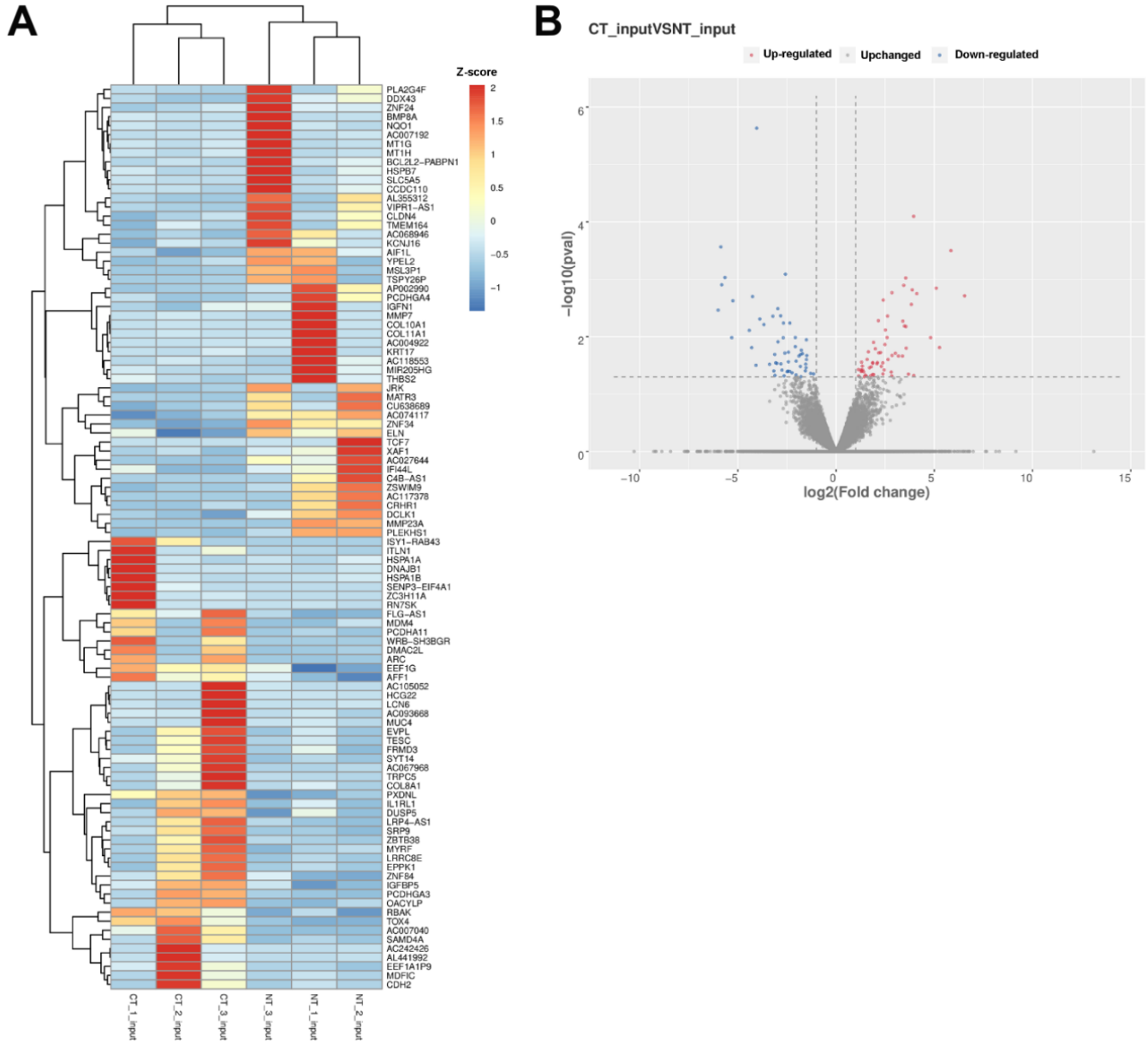


**Fig. 5: Analysis of DEGs between Cancer tissue and Normal tissue in PTC patients.**
A, Heatmap of the 123 DEGs in the Cancer tissue compared with Normal tissue. B, Volcano map of intersecting m6A signals for the 123 DEGs showing the distribution of genes that were upregulated, down-regulated or did not change


**Fig. 6: Enrichment analysis of DEGs.**

A, The enriched GO terms for the validated differentially methylated genes in the three categories of cellular component, molecular function, and biological process. B, The enriched KEGG pathways for the validated differentially methylated genes showing that they are related to were related to protein digestion and absorption, linoleic acid metabolism, legionellosis and alpha-linolenic acid metabolism. GO, gene ontology; KEGG: Kyoto Encyclopedia of Genes and Genomes

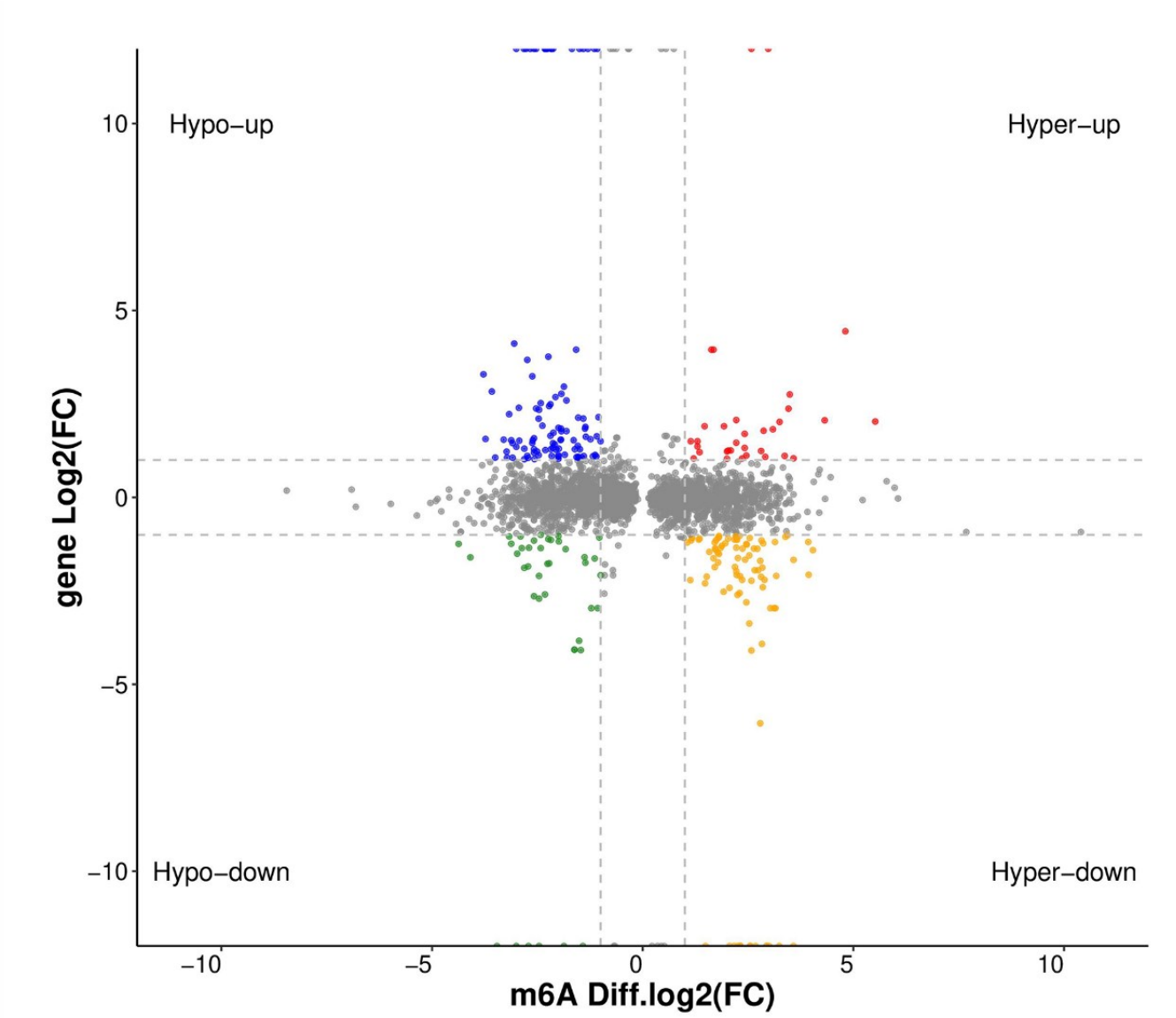


**Fig. 7: Four-quadrant diagram of m6A level and mRNA expression level.**
FC: fold change. The blue area represents genes whose m6A peak was down-regulated while their mRNA expression upregulated. The red area represents genes whose m6A peak and mRNA expression was upregulated. The green area represents genes whose m6A peak and mRNA expression was down-regulated. The yellow area represents genes whose m6A peak was upregulated, while their mRNA expression down-regulated

### *Construction and evaluation of prognostic risk model*

Genes that were upregulated at the m6A level but decreased at the transcription level and down-regulated at the m6A level but increased at the transcription level were screened as candidate genes. There were 153 genes matching these criteria, and their expression in the Primary Tumor and Solid tissue Normal tissues of TCGA database is shown via Heatmap in Fig. 8.

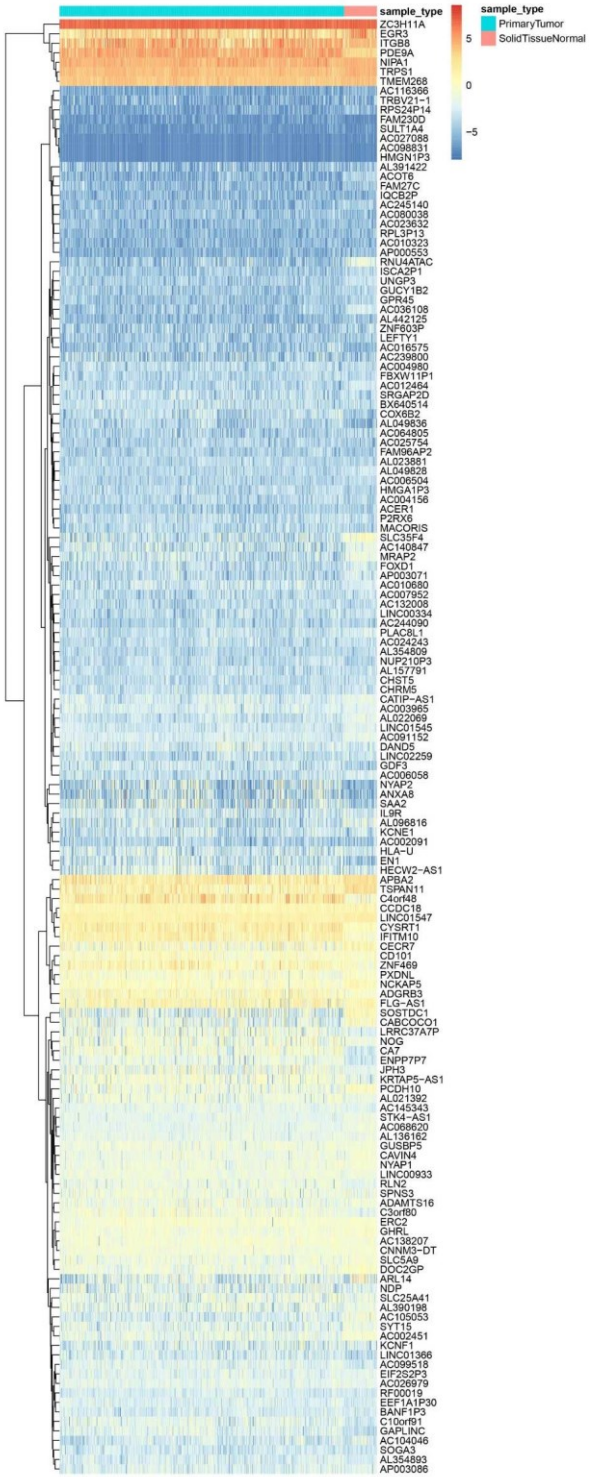


**Fig. 8:** The heatmap of the expression of 153 candidate genes in thyroid cancer (TCGA database) that were upregulated at the m6A level but decreased at the transcription level and down-regulated at the m6A level but increased at the transcription level

Next, we identified 36 corresponding genes by intersecting these genes with the immune-related genes downloaded from Immport, which were then entered into LASSO Cox regression analysis to compute the regression coefficient (Fig. 9A). Our results showed that the model achieved the best performance with the following 7 genes: *GDNF*, *EBI3*, *CCL2*, *BMP5*, *TGFB2*, *CGB3* and *RLN2* (Fig. 9B).

The 7 genes were screened and included in the multivariate risk model of coxph, and based on their corresponding risk score. These 7 genes were used to construct the m6A-related risk signature via multivariate CoxPH regression model (Table 2). Risk scores of patients were calculated as follows: Risk score = (-0.131054**GDNF*)+(-0.304905**EBI3*)+(0.373192**CCL2*)+(0.302847**BMP5*)+(0.168305**TGFB2*)+(0.257656**CFB3*)+(-0.459494**RLN2*). The PTC tissues from the TCGA database were classified into a low-risk and a high-risk group. The risk score distribution, survival state and expression levels of the 7 genes are shown in Fig. 9C. Further, Kaplan Meier survival analysis showed that the low-risk patients had superior overall survival (OS) than the high-risk patients (Fig. 9D, $P$=0.002). ROC curve analysis showed that the area under the curve (AUC) for 3-, 5- and 10-year overall survival of the model incorporating these 7 genes were 0.741, 0.709 and 0.691, respectively, demonstrating that this risk model has promising good prognostic ability in PTC (Fig. 9E).

**Table 2:** The multivariate Cox coefficients of 7 genes

| *Gene* | *Coef* | *HR* | *HR.95L* | *HR.95H* | *P Value* |
|---|---|---|---|---|---|
| *GDNF* | -0.131054 | 0.7636 | 0.4723 | 1.1242 | 0.0325 |
| *EBI3* | -0.304905 | 0.5896 | 0.3219 | 0.8927 | 0.0193 |
| *CCL2* | 0.373192 | 1.0514 | 0.6913 | 1.3291 | 0.0204 |
| *BMP5* | 0.302847 | 0.9772 | 0.7185 | 1.2037 | 0.0096 |
| *TGFB2* | 0.168305 | 0.8298 | 0.5344 | 1.0926 | 0.0007 |
| *CGB3* | 0.257656 | 1.1528 | 0.8249 | 1.3925 | 0.0105 |
| *RLN2* | -0.459494 | 0.5356 | 0.2655 | 0.7953 | 6.41e−05 |

## Discussion

MeRIP-seq allows the description of RNA methylation on a genome-wide scale via high-throughput sequencing technology (5). Mining RNA methylation patterns from MeRIP-seq high-throughput data can help reveal the potential functions of mRNA methylation in regulating gene expression and splicing, and effectively guide cancer intervention and treatment (5,11). This article clarifies the function of m6A in thyroid cancer through MeRIP-seq technology.

The distribution of m6A peaks was highly enriched near the transcription start site, and we screened out 1,417 genes with differences in m6A. Further screening identified 123 DEGs that were related to linoleic acid (LA) metabolism, α-linoleic acid metabolism, and protein digestion and absorption through functional analysis. Studies have shown that polyunsaturated fatty acids have a variety of biological activities in the body (12,13). They can not only serve as energy donors for cell metabolism, but also regulate cell membranes' composition and fluidity, affect cell mitochondria's function, and regulate cell growth. Many epidemiological and animal and cell experiments have confirmed that polyunsaturated fatty acids and their metabolic derivatives could regulate the activity of cancer without affecting normal cell activity (14,15). ALA and LA are two common unsaturated fatty acids in human free fatty acids.

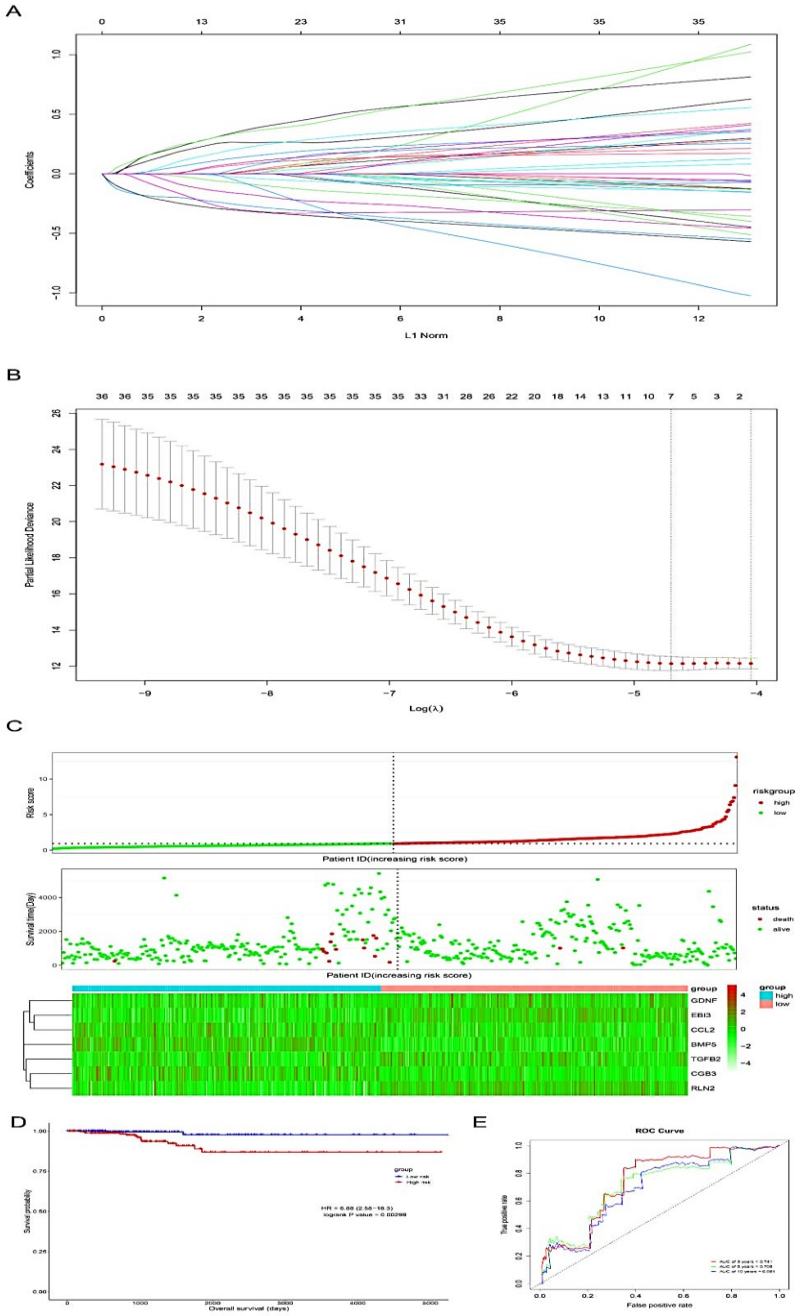


**Fig. 9: Survival prognosis model of the 7 genes in TCGA PTC cohort.**

A, LASSO coefficient profiles of the 36 genes related to the overall survival of PTC patients after intersecting the 153 candidate genes from Figure 8 with the immune-related genes downloaded from Immport website. B, Coefficient profile plot against the log (lambda) sequence in the LASSO model showing that it achieved the best performance with the 7 genes *GDNF*, *EBI3*, *CCL2*, *BMP5*, *TGFB2*, *CGB3* and *RLN2*. C, The distributions of the risk score, survival status, and expression profiles of the seven genes (*GDNF*, *EBI3*, *CCL2*, *BMP5*, *TGFB2*, *CGB3* and *RLN2*) in the high- and low-risk groups. D, Kaplan-Meier survival curves for overall survival of thyroid cancer patients in high- and low-risk groups from TCGA dataset (*P*=0.00299). E, ROC curve for predicting 3 (AUC=0.741), 5 (AUC=0.709) and 10 years (AUC=0.691) survival based on the risk score. TCGA: The Cancer Genome Atlas. ROC: Receiver operating characteristic curve. AUC: Area Under Curve

It was reported that ALA and LA could induce the accumulation of the toxic product α-lactalbumin in non-small cell lung cancer cells to cause cell apoptosis (16). Kyung Mee Kim et al. showed that the concentration of LA in the urine of thyroid cancer patients was significantly lower than normal controls (17). Combined with our results, it can be inferred that ALA and LA may exert a crucial regulatory effect in the progression of thyroid cancer, but the specific regulatory mechanism needs to be further explored.

Another enrichment pathway is protein digestion and absorption, which is one of the key ways to participate in cancer regulation. Through bioinformatics analysis, protein digestion and absorption pathways are related to lung metastasis in patients with osteosarcoma (18). Through RNA sequence analysis, Li-Feng Dong et al. found that genes related to protein digestion and absorption in breast cancer patients with lymphatic metastasis were significantly upregulated (19). Similar findings were also reported hat DEGs in Hispanic American childhood leukemia were related to protein digestion and absorption (20). However, there are very few studies on protein digestion and absorption in thyroid cancer, which is worthy of more attention.

This study identified a risk model consisting of 7 genes has prognostic value for thyroid cancer patients. The analysis shows that the model is related to the survival rate with good prognostic ability. *GDNF* is a highly conservative neurotrophic factor that can activate the downstream cell survival and proliferation signaling pathway and then promote the growth of thyroid cancer (21). Although there is no report about the participation of *EBI3* in the development of thyroid cancer, *EBI3* was shown to be related to the development of pancreatic cancer (22), and the specific mechanism may be related to the participation of *EBI3* in the immune function of Treg cells (23). *CCL2* is a chemokine, which was found to be related to lymph node metastasis in PTC patients, and its high expression is characteristic of recurrent PTC patients (24). Although there is few data about *BMP5* in thyroid cancer, recent research suggested that BMP5 seems to be related to thyroid activation (25). *TGFB2* can activate the TGF-β pathway, promote the epithelial-mesenchymal transformation of cancer cells (26). However, the direct relationship between TGFB2 and thyroid cancer remains to be studied. Currently, *CGB3* is only found to be related to the development of cervical cancer and ovarian cancer (27, 28). *RLN2*, a relaxin, has been shown to enhance the carcinogenic potential of thyroid cancer cells by upregulating matrix metalloproteinases (29). Overall, these seven genes are all related to cancer development, and most of them have been confirmed to be involved in the thyroid cancer progression. In addition, the results based on the ROC curve showed that these seven genes had good predictive ability of the 3-, 5- and 10-year survival rates of patients with thyroid cancer, and after further validation, could be considered for estimating thyroid cancer patients' survival to better determine which group of patients would require more aggressive treatment (high-risk group) while other lesser aggressive and close follow-up (low-risk group).

This study had some limitations. The number of cases in this study was small, and we only performed biological information analyses without further *in vitro* and *in vivo* validation to confirm the possible molecular mechanism.

## Conclusion

We revealed the enrichment pathway and function of m6A methylation genes in thyroid cancer and reported seven genes, *GDNF*, *EBI3*, *CCL2*, *BMP5*, *TGFB2*, *CGB3* and *RLN2*, that could be used to predict thyroid cancer prognosis.

## Journalism Ethicas considerations

Ethical issues (Including plagiarism, informed consent, misconduct, data fabrication and/or falsification, double publication and/or submission, redundancy, etc.) have been completely observed by the authors.

## Acknowledgements

This work was supported by The Construction Fund of Medical Key Disciplines of Hangzhou ( Project No. 20200486).

## Conflict of Interest

The authors declare that there is no conflict of interest.

## References

1. Wang J, Yu F, Shang Y, Ping Z, Liu L (2020). Thyroid cancer: incidence and mortality trends in China, 2005-2015. *Endocrine,* 68(1):163-173.
2. Zhou Z, Liu H, Yang Y, et al (2022). The five major autoimmune diseases increase the risk of cancer: epidemiological data from a large-scale cohort study in China. *Cancer Commun (Lond),* 42(5):435-446.
3. Jillard CL, Scheri RP, Sosa JA (2015). What Is the Optimal Treatment of Papillary Thyroid Cancer? *Adv Surg,* 49:79-93.
4. McLeod DS, Sawka AM, Cooper DS (2013). Controversies in primary treatment of low-risk papillary thyroid cancer. *Lancet,* 381(9871):1046-57.
5. Zhu W, Wang JZ, Xu Z, et al (2019). Detection of N6-methyladenosine modification residues (Review). *Int J Mol Med,* 43(6):2267-2278.
6. Meyer KD, Jaffrey SR (2017). Rethinking m(6)A Readers, Writers, and Erasers. *Annu Rev Cell Dev Biol,* 33:319-342.
7. He L, Li H, Wu A, Peng Y, Shu G, Yin G (2019). Functions of N6-methyladenosine and its role in cancer. *Mol Cancer,* 18(1):176.
8. Sun T, Wu R, Ming L (2019). The role of m6A RNA methylation in cancer. *Biomed Pharmacother,* 112:108613.
9. Xiang M, Liu W, Tian W, You A, Deng D (2020). RNA N-6-methyladenosine enzymes and resistance of cancer cells to chemotherapy and radiotherapy. *Epigenomics,* 12(9):801-809.
10. Chen X, Xu M, Xu X, et al (2020). METTL14 Suppresses CRC Progression via Regulating N6-Methyladenosine-Dependent Primary miR-375 Processing. *Mol Ther,* 28(2):599-612.
11. Dominissini D, Moshitch-Moshkovitz S, Schwartz S, et al (2012). Topology of the human and mouse m6A RNA methylomes revealed by m6A-seq. *Nature,* 485(7397):201-6.
12. Lee JM, Lee H, Kang S, Park WJ (2016). Fatty Acid Desaturases, Polyunsaturated Fatty Acid Regulation, and Biotechnological Advances. *Nutrients,* 8(1):23.
13. Massey KA, Nicolaou A (2011). Lipidomics of polyunsaturated-fatty-acid-derived oxygenated metabolites. *Biochem Soc Trans,* 39(5):1240-6.
14. Gorjao R, Dos Santos CMM, Serdan TDA, et al (2019). New insights on the regulation of cancer cachexia by N-3 polyunsaturated fatty acids. *Pharmacol Ther,* 196:117-134.
15. Huang M, Narita S, Koizumi A, et al (2021). Macrophage inhibitory cytokine-1 induced by a high-fat diet promotes prostate cancer progression by stimulating tumor-promoting cytokine production from tumor stromal cells. *Cancer Commun (Lond),* 41(5):389-403.
16. Zhang M, Yang F Jr, Yang F, et al (2009). Cytotoxic aggregates of alpha-lactalbumin induced by unsaturated fatty acid induce apoptosis in tumor cells. *Chem Biol Interact,* 180(2):131-42.
17. Kim KM, Jung BH, Lho DS, et al (2003). Alteration of urinary profiles of endogenous steroids and polyunsaturated fatty acids in thyroid cancer. *Cancer Lett,* 202(2):173-9.
18. Shi ZJ, Zhou HX, Pan B, et al (2017). Exploring the key genes and pathways of osteosarcoma with pulmonary metastasis using a gene expression microarray. *Mol Med Rep,* 16(5):7423-7431.
19. Dong LF, Xu SY, Long JP, Wan F, Chen YD (2017). RNA-Sequence Analysis Reveals Differentially Expressed Genes (DEGs) in Patients Exhibiting Different Risks of Tumor Metastasis. *Med Sci Monit,* 23:2842-2849.
20. Hsu LI, Briggs F, Shao X, et al (2016). Pathway Analysis of Genome-wide Association Study in Childhood Leukemia among Hispanics. *Cancer Epidemiol Biomarkers Prev,* 25(5):815-22.
21. Mulligan LM (2019). GDNF and the RET Receptor in Cancer: New Insights and Therapeutic Potential. *Front Physiol,* 9:1873.
22. Michaud D, Mirlekar B, Bischoff S, et al (2020). Pancreatic cancer-associated inflammation

drives dynamic regulation of p35 and Ebi3. *Cytokine,* 125:154817.
23. Faustino LD, Griffith JW, Rahimi RA, et al (2020). Interleukin-33 activates regulatory T cells to suppress innate γδ T cell responses in the lung. *Nat Immunol,* 21(11):1371-1383.
24. Tanaka K, Kurebayashi J, Sohda M, et al (2009). The expression of monocyte chemotactic protein-1 in papillary thyroid carcinoma is correlated with lymph node metastasis and tumor recurrence. *Thyroid,* 19(1):21-5.
25. Houtman E, Tuerlings M, Suchiman HED, et al (2022). Inhibiting thyroid activation in aged human explants prevents mechanical induced detrimental signalling by mitigating metabolic processes. *Rheumatology (Oxford),* 62(1):457-466.
26. Song C, Zhou C (2021). HOXA10 mediates epithelial-mesenchymal transition to promote gastric cancer metastasis partly via modulation of TGFB2/Smad/METTL3 signaling axis. *J Exp Clin Cancer Res,* 40(1):62.
27. Śliwa A, Kubiczak M, Szczerba A, et al (2019). Regulation of human chorionic gonadotropin beta subunit expression in ovarian cancer. *BMC Cancer,* 19(1):746.
28. Singh P, Chalertpet K, Sukbhattee J, et al (2022). Association between promoter methylation and gene expression of CGB3 and NOP56 in HPV-infected cervical cancer cells. *Biomed Rep,*16(1):1.
29. Bialek J, Kunanuvat U, Hombach-Klonisch S, et al (2011). Relaxin enhances the collagenolytic activity and in vitro invasiveness by upregulating matrix metalloproteinases in human thyroid carcinoma cells. *Mol Cancer Res,* 9(6):673-87.